EFFECTS OF CHEMICAL AND PHYSICAL MODELS ON A ONE-DIMENSIONAL FLOW IN A ROCKET NOZZLE

Luciano Kiyoshi Araki

Numerical Methods in Engineering Post-graduation Course
Federal University of Paraná
Curitiba, PR, Brazil
lucaraki@demec.ufpr.br

Carlos Henrique Marchi

Department of Mechanical Engineering
Federal University of Paraná
Caixa postal 19040
81531-980, Curitiba, PR, Brazil
marchi@demec.ufpr.br

Abstract: *a one-dimensional mathematical and numerical model for the flow in a LOX/LH_2-rocket engine nozzle is presented. Temperature is used as unknown at energy equation and velocity is obtained for all speeds regimes. For all analyses, tiny tolerances and a large number of iterations were used, in order to achieve the round-off error and estimate the discretization error. For each physical model, different chemical schemes are compared (among them and to reference ones, with good accuracy), indicating the influence of the choice of such schemes on numerical results. Six-species models and 80 control volumes are recommended, at least, for preliminary tests.*

1 Nomenclature

C_d	discharge coefficient
c_p	specific heat at constant pressure
$(c_p)_f$	frozen specific heat at constant pressure
F^*	non-dimensional momentum thrust
GCI	Grid Convergence Index
h_i	entalphy of species i
L	number of chemical reactions
$\dot{m}$	mass flow rate
M	molecular weight of the gases mixture
M_{ex}	Mach number at nozzle exit
N	total number of species in the flow
OF	oxidant/fuel ratio
P	pressure
P'	pressure correction
p_L	asymptotic order of the error
p_U	apparent order of the uncertainty
r	grid refinement ratio
R	gas constant or gases mixture constant
S	cross-section area
T	temperature
u	velocity
$\dot{w}$	mass generation rate
Y	mass fraction

Greek symbols

γ	ratio between specific heats
ρ	density

Subscripts

ex	nozzle exit
i	chemical species i

2 Introduction

For the design of a rocket engine, the first step is concerned about modelling the combustion gases flow. Although two and three-dimensional models are commonly used, one-dimensional models are still employed in rocket engines projects, being corrected by empirical coefficients (Fröhlich et al., 1993; Sutton and Biblarz, 2001). Studies involving one-dimensional codes are, because of this, still useful.

The complete problem involving the combustion gases flow and the regenerative cooling system may be divided up into three sub-problems, namely: (1) the reactive combustion gases flow through the rocket engine; (2) the heat conduction from hot gases to the coolant, through the wall structure; and (3) the turbulent coolant flow, in the regenerative cooling system. In this work, only the first sub-problem, namely the reactive combustion gases flow, is studied.

For this study, however, different physical and chemical schemes are used. Five physical models are compared: one-species gas with constant or with variable properties; frozen, equilibrium and non-equilibrium flows. Otherwise, for these three last models, which include multi-species flows, chemical schemes are also considered. Results are compared with those obtained from CEA code, from NASA (GRS, 2005), and the analytical solution for quasi-one-dimensional isentropic flow. Differently from commonly used, the energy equation is based on temperature, and not on enthalpy nor internal energy (Barros, 1993; Dunn and Coats, 1997; Laroca, 2000); the velocity is obtained for the whole flow (from subsonic to supersonic regimes) and not only for supersonic flow (Barros, 1993; Dunn and Coats, 1997; Smith et al., 1987). And for all the analyses, numerical error estimates, based on GCI estimator (Roache, 1994), are also presented.

3 Mathematical model

The basic principles of rocketry are essentially those of mechanics, thermodynamics and chemistry (Sutton and Biblarz, 2001). In this way, the mathematical formulation for a single-species/multi-species flow through the nozzle engine is based only on four equations: conservation of mass, conservation of momentum, conservation of energy and state (the perfect gases law), given in the sequence:

$$\frac{d}{dx}\left(\rho\, u\, S\right) = 0\,, \tag{1}$$

$$\frac{d}{dx}\left(\rho\, u\, S\, u\right) = -S\frac{dP}{dx}\,, \tag{2}$$

$$(c_p)_f \frac{d}{dx}\left(\rho\, u\, S\, T\right) = u\, S\frac{dP}{dx} + S_{eq/ne}\,, \tag{3}$$

$$P = \rho\, R\, T\,, \tag{4}$$

where: ρ, u, P and T are four dependent variables, related to density, velocity, pressure and temperature (in this order); x is the axial coordinate; S is the cross-section area; R is the gas/mixture of gases constant; $(c_p)_f$ is the frozen specific heat at constant pressure; and $S_{eq/ne}$ is a source term taken only into account for equilibrium or non-equilibrium flows and is evaluated by:

$$S_{eq/ne} = \begin{cases} -\sum_{i=1}^{N} h_i \frac{d}{dx}\left(\rho\, u\, S\, Y_i\right), & \text{for local equilibrium flow;} \\ -S\sum_{i=1}^{N} h_i \dot{w}_i\,, & \text{for non-equilibrium flow;} \end{cases} \tag{5}$$

where: N is the total number of species existent in the flow; h_i is the enthalpy for each chemical species i; Y_i is the mass fraction for each chemical species i; and $\dot{w}_i$ corresponds to mass generation rate of species i.

As can be seen above, the conservation of energy, Eq. (3), has the temperature as unknown and not the enthalpy nor the internal energy, as normally used (Barros, 1993; Dunn and Coats, 1997; Laroca, 2000). The major advantage of such variation is on the temperature determination, which is obtained directly from the numerical model, not depending on the enthalpy (or internal energy) values.

Equations (1) to (4) are enough for the mathematical formulation of one-species, frozen and equilibrium flows. For non-equilibrium model, however, associated to these four equations must be taken into account the continuity equation for species *i*:

$$\frac{d}{dx}\left(\rho\, u\, S\, Y_i\right) = S\, \dot{w}_i\,, \tag{6}$$

which corresponds to the conservation of mass for each species separately. The mass generation rate of species, $\dot{w}_i$, depends on the forward reaction constants, mass concentration of species and efficiencies of 3rd body species (on a given reaction).

Chemical equilibrium composition, for frozen and local equilibrium flows, is obtained by equilibrium constants, as explained at (Kuo, 1986). On the other hand, non-equilibrium chemical composition is obtained using the methodology of (Anderson, 1990; Barros et al., 1990; Kee et al., 1996). Some attention must be taken, otherwise, for the evaluation of the frozen specific heat at constant pressure and the ratio of specific heats (for equilibrium flow), which can be estimated by:

$$(c_p)_f = \sum_{i=1}^{N} Y_i (c_p)_i\,, \tag{7}$$

$$\gamma = \frac{1}{1 + \dfrac{P}{M}\displaystyle\sum_{i=1}^{N}\left[M_i\left(\frac{\partial X_i}{\partial P}\right)_T\right]} \cdot \frac{(c_p)_f}{(c_p)_f - \displaystyle\sum_{i=1}^{N} Y_i R_i}\,, \tag{8}$$

where: $(c_p)_i$ is the specific heat at constant pressure for each chemical species *i* in the control volume; *M* is the molecular weight for the gases mixture; X_i is the molar fraction; M_i is the molecular weight for the chemical species *i*; and R_i refers to gas constant for each single-species *i*.

Nine different chemical reaction schemes for frozen and equilibrium flows are presented, including from 3 to 8 chemical species and from 0 to 18 chemical reaction equations. Despite of this, a one-single-species gas flow is also studied, for constant and variable properties. For non-equilibrium flow, only six and eight-species models are studied, totalling six chemical reaction schemes. Table 1 shows a summary of the chemical reaction models implemented, in which *L* represents the number of chemical reaction equations. Even if two models have the same number of reactions and species, they differ at least for one chemical reaction. For non-equilibrium studies, model 3 was split up into two different non-equilibrium models, which differ from each other about the mass generation rates.

Table 1. Chemical reaction models implemented in Mach1D code.

Model	*L*	*N*	Species	Observations
0	0	3	H_2O, O_2, H_2	Ideal model
1	1	3	H_2O, O_2, H_2	–
2	2	4	H_2O, O_2, H_2, OH	–
3	4	6	H_2O, O_2, H_2, OH, O, H	4 reactions with 3rd body of Smith et al. (1987) and Barros et al. (1990)
4	4	6	H_2O, O_2, H_2, OH, O, H	4 reactions; model of Svehla (1964)
5	8	6	H_2O, O_2, H_2, OH, O, H	8 reactions (4 with 3rd body); model of Barros et al. (1990)
7	8	6	H_2O, O_2, H_2, OH, O, H	8 reactions (4 with 3rd body); model of Smith et al. (1987)
10	6	8	H_2O, O_2, H_2, OH, O, H, HO_2, H_2O_2	4 reactions from model 3 and 2 of Kee et al. (1990)
9	18	8	H_2O, O_2, H_2, OH, O, H, HO_2, H_2O_2	18 reactions (5 with 3rd body); model of Kee et al. (1990)

4 Numerical model

The mathematical model for combustion gases flow in the nozzle structure is discretized using a finite volume method. The domain is divided into *Nvol* control volumes, in which the differential equations are integrated: Eqs. (1) to (3), (5) and (6). A co-located grid arrangement, appropriated for all speed flows is used (Marchi and Maliska, 1994), associated with a second-order discretization scheme (CDS), with deferred correction (Ferziger and Peric, 2001). The system of algebraic equations obtained is solved by TDMA method (Ferziger and Peric, 2001).

Pressure and velocity are coupled by SIMPLEC algorithm (Van Doormaal and Raithby, 1984), in order to convert the mass equation in a pressure-correction one. So, the mass conservation equation, Eq. (1), is used for determination of a pressure-correction (P'), while velocity (u) is obtained from the momentum equation, Eq. (2), and the energy equation, Eq. (3), is taken for temperature (T) determination. Density (ρ) is got from the state equation, Eq. (4). It must be noted that velocity (u) is evaluated from very reduced values (near null values) until supersonic ones, and not only for supersonic values, as commonly found in literature (Barros, 1993; Dunn and Coats, 1997; Smith et al., 1987).

A basic algorithm for one-dimensional combustion gases flow is shown in the following.

Algorithm:

1. Definition of data (T, P, ρ, u) in an instant t, using the analytical solution for one-dimensional isentropic flow.
2. Estimation of all variables in an instant $t+\Delta t$ (the integration of all the equations is based on a completely implicit formulation; time, however, is used only as a relaxation parameter, once this work is taken for steady state flow).
3. Definition of thermophysical properties (such as the c_p, γ and R).
4. Estimation of the inlet pressure and the inlet velocity.
5. Coefficients calculation for the algebraic system (by discretization) of the momentum equation and solution of this system by TDMA for u.
6. Calculation of SIMPLEC coefficients.
7. Estimation of face velocities.
8. Estimation of the inlet temperature at the nozzle engine.
9. Coefficients calculation for the algebraic system (by discretization) of the energy equation and solution by TDMA for T.
10. Calculation of density (both, inside the control volumes and at their faces).
11. Coefficients calculation for the algebraic system (by discretization) of the mass equation and solution by TDMA for P'.
12. Correction of nodal pressures, face and nodal densities and face and nodal velocities by P'.
13. Return to item 2, until the achievement of the desired number of iterations.
14. Post-processing.

Over this basic algorithm, some modifications are necessary, depending on the physical model. For isentropic one-species gas with constant properties, for example, item 3 is unnecessary because all the thermochemical properties must be supplied as initial data. For a frozen flow, however, item 3 includes chemical composition determination for the first control volume (and the same chemical composition is maintained for all other volumes); in this case, also, the thermoproperties must be re-evaluated for every single control volume.

When the equilibrium flow model is studied, item 3 includes the chemical composition determination for all control volumes and, also here, the determination of thermoproperties must be done for every single control volume. And for non-equilibrium flow, this same item includes the mass generation rate determination and the use of Eq. (6), in order to estimate the chemical composition.

The boundary conditions adopted for the combustion gases flow are:

- Inlet conditions: temperature (T) and pressure (P) are functions of stagnation conditions; the chemical mixture composition, given by mass fractions (Y_i), is obtained from local data (temperature and pressure); this is not necessary for one-species models. The inlet velocity (u) is obtained from a linear extrapolation from internal control volumes.
- Nozzle walls: adiabatic.
- Exit conditions: for supersonic flows in nozzles, no exit boundary conditions are required. For the implementation of a numerical model, however, exit boundary conditions are needed. Because of this,

temperature (T), velocity (u), pressure (P) and mass fractions (Y_i) are obtained by linear extrapolation from internal control volumes.

5 Definition of the problem

The rocket engine geometry used in this work is the same one presented in (Marchi et al., 2000 and 2004), which consists on a cylindrical section, called combustion chamber (with radius r_{in} and length Lc) assembled to a nozzle device, whose longitudinal section is defined by a cosine curve (with throat nozzle radius r_g and length Ln). The radius r, for $x > Lc$, is evaluated by the following equation:

$$r = r_g + \frac{(r_{in} - r_g)}{2}\left\{1 + \cos\left[2\pi\frac{(x - Lc)}{Ln}\right]\right\}, \tag{9}$$

where x corresponds to the position where the radius is evaluated. Despite the cylindrical section is called combustion chamber, it does not correspond to a real combustion chamber; the effects of fuel and oxidant injection, mixture and burning are not considered. Fig. 1 shows all geometrical parameters of the nozzle studied in this work.

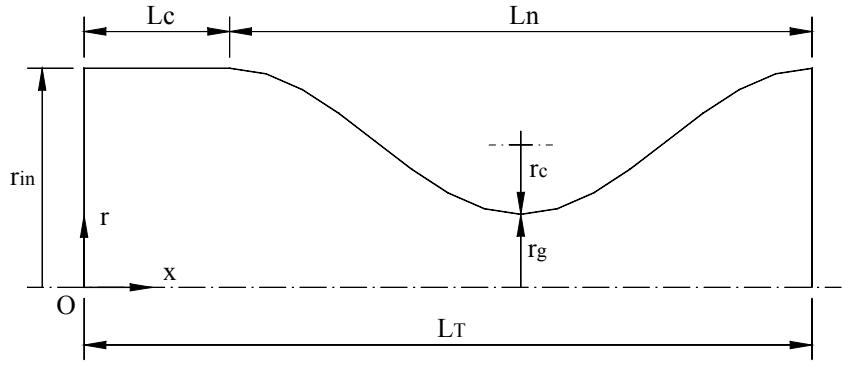

Figure 1. Geometrical parameters of the nozzle.

Some parameters of interest taken into account in this work are the nozzle discharge coefficient and the non-dimensional momentum thrust. Both of them are global parameters and evaluate how much the experimental values (laboratorial or numerical ones) are distant from theoretical values (obtained from one-dimensional isentropic flow analysis). In this work, however, the experimental values are always related to numerical results and theoretical ones are obtained from quasi-one-dimensional analytical solution.

The nozzle discharge coefficient (C_d) is defined as the ratio between experimental mass flow rate and the theoretical one, given by

$$C_d = \frac{\dot{m}_{\text{experimental}}}{\dot{m}_{\text{theoretical}}}, \tag{10}$$

where $\dot{m}$ corresponds to the mass flow rate.

Another parameter of interest is the non-dimensional momentum thrust (F^*), which is defined by the ratio between experimental and theoretical thrusts, given by

$$F^* = \frac{F_{\text{experimental}}}{F_{\text{theoretical}}}, \tag{11}$$

where F corresponds to the thrust values and, for ideal cases (in which the exit and ambient pressures are equal) can be obtained by the following relation, where u_{ex} is the exit velocity:

$$F = \dot{m}\, u_{ex}. \tag{12}$$

For this work, the combustion chamber total length (L_T) is equal to 0.5 m, in which 0.1 m is related to combustion chamber length (Lc) and the nozzle length (Ln) is 0.4 m. The nozzle entrance radius (r_{in}) is 0.3 m,

while the nozzle throat radius (r_g) is 0.1 m. Stagnation temperature is taken as 3420.33 K, while stagnation pressure is equal to 2.0 Mpa. The ratio between specific heats (γ) is 1.1956, the gas constant (R) is 526.97 J/kg^{x}K and the oxidant/fuel ratio is taken as the stoichoimetric one (OF = 7.936682739).

6 Numerical results and discussion

Five different physical models (isentropic one-species flow with constant properties; isentropic one-species flow with variable properties; frozen flow; local equilibrium flow; and non-equilibrium flow), associated to six (for non-equilibrium flow) or nine chemical reaction schemes (for frozen and local equilibrium flows) were implemented in Mach1D code, using FORTRAN 95 language and Compaq 6.6 compiler. For all the analyses, a PC, with Pentium IV 2.4 GHz processor, 1 GB RAM was used; exception was made for local equilibrium and non-equilibrium flow analyses, for which a PC, with Pentium IV 3.4 GHz processor, 4 GB RAM was employed.

6.1 Numerical error: GCI estimator

For one-species models and the frozen flow one, the simulations were made for 11 different grids, to allow the determination of apparent and effective convergence orders (Marchi and Silva, 2002). Numerical error estimates, also, based on GCI estimator (Roache, 1994), were taken for all the physical and chemical models. Some pieces of information about numerical errors and error estimators can be found in (Tannehill et al., 1997; Marchi, 2001; Ferziger and Peric, 2001). Error estimates are very important for evaluating if two different physical (or chemical) models have the same results or the differences can be assigned to numerical errors.

The GCI estimator is evaluated by

$$GCI(\varphi_1, p) = 3\frac{|\varphi_1 - \varphi_2|}{(r^p - 1)}, \tag{13}$$

where: φ_1 and φ_2 are, respectively, the numerical solutions for the fine (h_1) and coarse (h_2) grids; r is the grid refinement ratio ($r = h_2 / h_1$); h is the grid spacing or distance between two successive grid points; and p is related to the asymptotic (p_L) or apparent (p_U) order (the lowest value between the two ones). Asymptotic order depends on the chosen discretization model, while apparent order, for constant refinement ratio, is evaluated by

$$p_U(h_1) = \frac{\log\left(\dfrac{\varphi_2 - \varphi_3}{\varphi_1 - \varphi_2}\right)}{\log(r)}. \tag{14}$$

where φ_3 corresponds to the numerical solution for a supercoarse grid.

6.2 CPU time

In a numerical study, both results and CPU time consumption are of great importance. In all analyses, the number of iterations was high enough for achieving the round-off error and the tolerance of 10^{-12} for chemical composition determination from 5.0×10^3 up to 1.2×10^9 outer iterations were necessary, depending on the grid refinement and/or the physical and chemical models. This was necessary to minimize other types of numerical errors than discretization ones and, in this way, to guarantee that numerical errors are made, essentially, of discretization ones.

Taking constant or variable properties influences the CPU time, especially for refined grids. Comparing the CPU time for 2560 control volumes, both with 80,000 iterations, the time spent for variable properties model is about 50% greater than for constant properties: 3.0 min against 2.1 min. For the frozen flow model, with 80 control volumes, all the chemical reaction models show similar time requirements, with CPU time between 0.92 s (models 1 and 9) and 0.98 s (models 0 and 2). For the local equilibrium flow, otherwise, for the same grid, simulations can take less than 3 s (models 0, 1 and 2), between 1.5 and 3 min (models 3, 4 and 10) or hours (models 5, 9 and 7), depending on the chosen chemical scheme. Similar behaviour is seen for non-equilibrium flow. Only one study could not be finished, by time restrictions: the model 9 for non-equilibrium flow, after running five days (and 1.2×10^9 iterations), achieved only one significant figure.

Even chemical reaction schemes that present exactly the same chemical species have unequal CPU time performances. While equilibrium flow simulations using models 3 and 4 (both with four chemical reaction equations) take less than 3 minutes, for 80 control volumes, the same simulations with models 5 and 7 (both with

eight equations) take more than 4 hours, at least 120 times more. Besides, models 3 and 4 have higher performances for local equilibrium models and they also present a greater quantity of significant figures (about 11), when compared to models 5 and 7 (which present about 8). The same phenomenon takes place to chemical models 9 (18 reaction equations) and 10 (6 equations) and for non-equilibrium models. A possible explanation for this event takes into account the number of chemical reaction equations: the larger the amount of equations, the greater the time necessary for convergence (and also, because of the larger amount of iterations needed, the truncations errors become greater and the quantity of significant figures decreases).

6.3 Chemical composition

Table 2 contain information about the mixture of the combustion gases (H_2O, O_2 and H_2 mass fractions) at the nozzle exit, for frozen, local equilibrium and non-equilibrium flows (respectively). It can be noted that, for each physical model, six and eight-species models have the closest results to CEA (which takes into account nine species, the same eight from models 9 and 10, including also ozone, O_3).

For frozen flow, the chemical composition is kept the same over all the flow. However, for local equilibrium flow, the composition must be recalculated at each control volume. Because of this, each chemical reaction scheme presents a different mass fraction profile. Figure 2 shows the H_2O mass fraction profile for different chemical schemes implemented at Mach1D code. Again, the chemical reaction schemes that have better results are the six-species and eight-species models. Otherwise, not only for H_2O mass fraction profile, but also for other species are the results obtained from Mach1D close to those ones from CEA.

Table 2. Mass fractions at the nozzle exit with 80 control volumes.

Model	Frozen flow			Equilibrium flow			Model	Non-equilibrium flow		
	H_2O	O_2	H_2	H_2O	O_2	H_2		H_2O	O_2	H_2
0	1.00000	0.00000	$7x10^{-13}$	1.00000	0.00000	$7x10^{-13}$	**31**	0.81253	0.10023	0.01709
1	0.87442	0.11153	0.01405	0.98257	0.01548	0.00195	**32**	0.82375	0.09475	0.01600
2	0.80422	0.07703	0.01581	0.95413	0.02494	0.00414	**5**	0.86178	0.07762	0.01102
3, 4, 5, 7	0.78369	0.07754	0.01565	0.92742	0.03659	0.00606	**7**	0.86811	0.07282	0.01059
9, 10	0.78354	0.07743	0.01565	0.92736	0.03661	0.00606	**10**	0.81247	0.10022	0.01709
CEA	0.77987	0.07515	0.01570	0.92548	0.03579	0.00611				

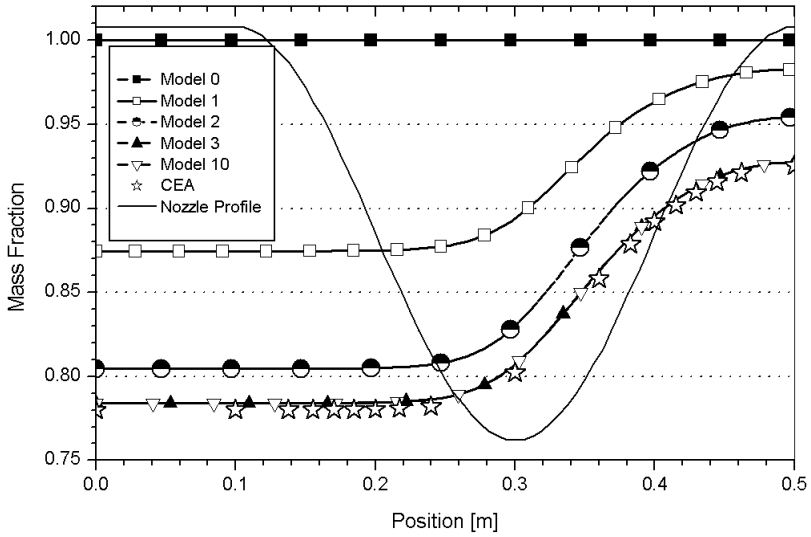

Figure 2. H_2O mass fraction profiles along the nozzle, for local equilibrium flow with 80 control volumes.

6.4 Parameters of interest

Tables 3 and 4 supply numerical results for all the analyses made, including numerical error estimates by GCI estimator, for 80 control volumes. Taking into account the numerical error estimates, it can be seen that both six-species and eight-species models present the same numerical results and also, include CEA results, for frozen flow model. Similar results were obtained for local equilibrium flow; the six-species and eight-species Mach1D results, however, do not include CEA ones for all the variables, although they are close to each other (the differences are below 3%). Based on this, both six and eight-species models seem to be the most adequate ones for studies involving frozen and/or local equilibrium flow.

Table 3. C_d, F^* and P_{ex} with 80 control volumes.

Model	C_d [adim.]	F^* [adim.]	P_{ex} [Pa]
Analytical (R1)	**1.0**	**1.0**	**2.917342×10^4**
Constant Properties (R1)	$1.000 \pm 3 \times 10^{-3}$	$1.001 \pm 4 \times 10^{-3}$	$2.912 \times 10^4 \pm 8 \times 10^1$
Variable Properties (R1)	$0.992 \pm 3 \times 10^{-3}$	$1.004 \pm 4 \times 10^{-3}$	$3.005 \times 10^4 \pm 7 \times 10^1$
Variable Properties (R2)	$1.060 \pm 3 \times 10^{-3}$	$1.004 \pm 4 \times 10^{-3}$	$3.005 \times 10^4 \pm 7 \times 10^1$
Frozen Flow – mod. 0	$1.060 \pm 3 \times 10^{-3}$	$1.004 \pm 4 \times 10^{-3}$	$3.005 \times 10^4 \pm 7 \times 10^1$
Frozen Flow – mod. 1	$1.032 \pm 3 \times 10^{-3}$	$1.002 \pm 4 \times 10^{-3}$	$2.886 \times 10^4 \pm 9 \times 10^1$
Frozen Flow – mod. 2	$1.018 \pm 3 \times 10^{-3}$	$1.001 \pm 4 \times 10^{-3}$	$2.81 \times 10^4 \pm 1 \times 10^2$
Frozen Flow – mod. 3, 4, 5 and 7	$1.001 \pm 3 \times 10^{-3}$	$1.000 \pm 4 \times 10^{-3}$	$2.74 \times 10^4 \pm 1 \times 10^2$
Frozen Flow – mod. 9 and 10	$1.001 \pm 3 \times 10^{-3}$	$1.000 \pm 4 \times 10^{-3}$	$2.74 \times 10^4 \pm 1 \times 10^2$
CEA (frozen flow)	**1.000580**	**0.998992**	**2.7448×10^4**
Equilibrium Flow – mod. 0	$1.060 \pm 9 \times 10^{-3}$	$1.00 \pm 1 \times 10^{-2}$	$3.005 \times 10^4 \pm 7 \times 10^1$
Equilibrium Flow – mod. 1	$1.02 \pm 1 \times 10^{-2}$	$1.01 \pm 1 \times 10^{-2}$	$3.37 \times 10^4 \pm 3 \times 10^2$
Equilibrium Flow – mod. 2	$1.00 \pm 1 \times 10^{-2}$	$1.01 \pm 1 \times 10^{-2}$	$3.54 \times 10^4 \pm 5 \times 10^2$
Equilibrium Flow – mod. 3, 4, 5 and 7	$0.98 \pm 1 \times 10^{-2}$	$1.01 \pm 1 \times 10^{-2}$	$3.63 \times 10^4 \pm 5 \times 10^2$
Equilibrium Flow – mod. 9 and 10	$0.98 \pm 1 \times 10^{-2}$	$1.01 \pm 1 \times 10^{-2}$	$3.63 \times 10^4 \pm 5 \times 10^2$
CEA (local equilibrium flow)	**0.977372**	**1.011553**	**3.6178×10^4**
Non-equilibrium Flow – mod. 31	$1.008 \pm 3 \times 10^{-3}$	$1.013 \pm 5 \times 10^{-3}$	$3.175 \times 10^4 \pm 7 \times 10^1$
Non-equilibrium Flow – mod 32	$1.007 \pm 3 \times 10^{-3}$	$1.014 \pm 5 \times 10^{-3}$	$3.254 \times 10^4 \pm 6 \times 10^1$
Non-equilibrium Flow – mod. 5	$1.007 \pm 3 \times 10^{-3}$	$1.015 \pm 5 \times 10^{-3}$	$3.359 \times 10^4 \pm 5 \times 10^1$
Non-equilibrium Flow – mod. 7	$1.007 \pm 3 \times 10^{-3}$	$1.015 \pm 5 \times 10^{-3}$	$3.433 \times 10^4 \pm 3 \times 10^1$
Non-equilibrium Flow – mod. 10	$1.008 \pm 3 \times 10^{-3}$	$1.013 \pm 5 \times 10^{-3}$	$3.175 \times 10^4 \pm 7 \times 10^1$

(R1): Rg = 526.97 J/kg·K; (R2): Rg ≈ 461.53 J/kg·K (equivalent to combustion gases mixture for the ideal model)

Table 4. T_{ex}, u_{ex} and M_{ex} with 80 control volumes.

Model	T_{ex} [K]	u_{ex} [m/s]	M_{ex} [adim.]
Analytical (R1)	**1712.7409**	**3316.7150**	**3.1928346**
Constant Properties (R1)	1710 ± 7	3319 ± 7	$3.20 \pm 1 \times 10^{-2}$
Variable Properties (R1)	1800 ± 7	3357 ± 7	$3.15 \pm 1 \times 10^{-2}$
Variable Properties (R2)	1800 ± 7	3142 ± 6	$3.15 \pm 1 \times 10^{-2}$
Frozen Flow – mod. 0	1800 ± 7	3142 ± 6	$3.15 \pm 1 \times 10^{-2}$
Frozen Flow – mod. 1	1713 ± 8	3221 ± 7	$3.19 \pm 1 \times 10^{-2}$
Frozen Flow – mod. 2	1660 ± 8	3262 ± 7	$3.21 \pm 1 \times 10^{-2}$
Frozen Flow – mod. 3, 4, 5 and 7	1606 ± 9	3312 ± 7	$3.24 \pm 1 \times 10^{-2}$
Frozen Flow – mod. 9 and 10	1606 ± 9	3312 ± 7	$3.24 \pm 1 \times 10^{-2}$
CEA (frozen flow)	**1607.91**	**3311.4519**	**3.231**
Equilibrium Flow – mod. 0	$1800 \pm 2 \times 10^1$	$3140 \pm 2 \times 10^1$	$3.15 \pm 3 \times 10^{-2}$
Equilibrium Flow – mod. 1	2171 ± 4	3282 ± 3	$2.998 \pm 6 \times 10^{-3}$
Equilibrium Flow – mod. 2	$2345.9 \pm 7 \times 10^{-1}$	$3354.3 \pm 1 \times 10^{-1}$	$2.9357 \pm 3 \times 10^{-4}$

Equilibrium Flow – mod. 3, 4, 5 and 7	$2461.2 \pm 3\text{x}10^{-1}$	3427 ± 2	$2.911 \pm 2\text{x}10^{-3}$
Equilibrium Flow – mod. 9 and 10	$2461.4 \pm 3\text{x}10^{-1}$	3427 ± 2	$2.911 \pm 2\text{x}10^{-3}$
CEA (local equilibrium flow)	**2462.41**	**3432.7056**	**2.986**
Non-equilibrium Flow – mod. 31	$1910 \pm 1\text{x}10^{1}$	3332 ± 6	$3.05 \pm 1\text{x}10^{-2}$
Non-equilibrium Flow – mod 32	$1980 \pm 1\text{x}10^{1}$	3338 ± 6	$3.02 \pm 1\text{x}10^{-2}$
Non-equilibrium Flow – mod. 5	2059 ± 9	3344 ± 6	$2.98 \pm 1\text{x}10^{-2}$
Non-equilibrium Flow – mod. 7	2117 ± 8	3344 ± 6	$2.96 \pm 1\text{x}10^{-2}$
Non-equilibrium Flow – mod. 10	$1910 \pm 1\text{x}10^{1}$	3332 ± 6	$3.05 \pm 1\text{x}10^{-2}$

(R1): Rg = 526.97 J/kg·K; (R2): Rg ≈ 461.53 J/kg·K (equivalent to combustion gases mixture for the ideal model)

Tables 5 and 6 supply numerical results for all the analyses made, including numerical error estimates by GCI estimator, for 2560 control volumes. These tables do not include results for non-equilibrium models 5, 7 and 10 (as well as equilibrium models 5, 7 and 9), due to time restrictions. As expected, the grid refinement provides better numerical results; exception is made for equilibrium temperature, for which with 80 control volumes present results closer to CEA than the ones obtained for 2560 control volumes. The differences between Mach1D and CEA results are, at maximum, of 0.28% for frozen flow and 2.5% for equilibrium flow, considering exit Mach number, using 80 control volumes; when 2560 control volumes are used, these differences drop to 0.08% for frozen flow and 2.4% for equilibrium flow. This reduction, however, is quite small, when compared to the larger CPU time consumption demanded by the grid refinement.

Table 5. C_d, F^* and P_{ex} with 2560 control volumes.

Model	C_d [adim.]	F^* [adim.]	P_{ex} [Pa]
Analytical (R1)	**1.0**	**1.0**	**29,173.42**
Constant Properties (R1)	$1.000000 \pm 1\text{x}10^{-6}$	$1.000000 \pm 1\text{x}10^{-6}$	$29{,}173.3 \pm 2\text{x}10^{-1}$
Variable Properties (R1)	$0.991754 \pm 1\text{x}10^{-6}$	$1.003224 \pm 1\text{x}10^{-6}$	$30{,}098.3 \pm 2\text{x}10^{-1}$
Variable Properties (R2)	$1.059739 \pm 1\text{x}10^{-6}$	$1.003224 \pm 1\text{x}10^{-6}$	$30{,}098.3 \pm 2\text{x}10^{-1}$
Frozen Flow – mod. 0	$1.059711 \pm 1\text{x}10^{-6}$	$1.003224 \pm 1\text{x}10^{-6}$	$30{,}098.6 \pm 2\text{x}10^{-1}$
Frozen Flow – mod. 1	$1.031887 \pm 1\text{x}10^{-6}$	$1.001341 \pm 1\text{x}10^{-6}$	$28{,}915.0 \pm 2\text{x}10^{-1}$
Frozen Flow – mod. 2	$1.017664 \pm 1\text{x}10^{-6}$	$1.000191 \pm 1\text{x}10^{-6}$	$28{,}201.0 \pm 2\text{x}10^{-1}$
Frozen Flow – mod. 3, 4, 5 and 7	$1.001086 \pm 1\text{x}10^{-6}$	$0.998981 \pm 1\text{x}10^{-6}$	$27{,}460.1 \pm 2\text{x}10^{-1}$
Frozen Flow – mod. 9 and 10	$1.001094 \pm 1\text{x}10^{-6}$	$0.998982 \pm 1\text{x}10^{-6}$	$27{,}460.7 \pm 2\text{x}10^{-1}$
CEA (frozen flow)	**1.000580**	**0.998992**	**27,448**
Equilibrium Flow – mod. 0	$1.059711 \pm 3\text{x}10^{-6}$	$1.003224 \pm 4\text{x}10^{-6}$	$30{,}098.6 \pm 6\text{x}10^{-1}$
Equilibrium Flow – mod. 1	$1.0190 \pm 1\text{x}10^{-4}$	$1.00884 \pm 1\text{x}10^{-5}$	$33{,}610 \pm 1\text{x}10^{1}$
Equilibrium Flow – mod. 2	$0.9986 \pm 1\text{x}10^{-4}$	$1.010751 \pm 8\text{x}10^{-6}$	$35{,}290 \pm 1\text{x}10^{1}$
Equilibrium Flow – mod. 3 and 4	$0.9782 \pm 1\text{x}10^{-4}$	$1.011582 \pm 8\text{x}10^{-6}$	$36{,}160 \pm 2\text{x}10^{1}$
Equilibrium Flow – mod. 10	$0.9782 \pm 1\text{x}10^{-4}$	$1.011587 \pm 8\text{x}10^{-6}$	$36{,}170 \pm 2\text{x}10^{1}$
CEA (local equilibrium flow)	**0.977372**	**1.011553**	**36,178**
Non-equilibrium Flow – mod. 31	$1.007717 \pm 2\text{x}10^{-6}$	$1.011741 \pm 1\text{x}10^{-6}$	$31{,}804.9 \pm 4\text{x}10^{-1}$
Non-equilibrium Flow – mod 32	$1.006824 \pm 5\text{x}10^{-6}$	$1.012647 \pm 1\text{x}10^{-6}$	$32{,}592.3 \pm 7\text{x}10^{-1}$

(R1): Rg = 526.97 J/kg·K; (R2): Rg ≈ 461.53 J/kg·K (equivalent to combustion gases mixture for the ideal model)

Table 6. T_{ex}, u_{ex} and M_{ex} with 2560 control volumes.

Model	T_{ex} [K]	u_{ex} [m/s]	M_{ex} [adim.]
Analytical (R1)	**1712.7409**	**3316.7150**	**3.1928346**
Constant Properties (R1)	$1712.739 \pm 7\text{x}10^{-3}$	$3316.717 \pm 7\text{x}10^{-3}$	$3.19284 \pm 1\text{x}10^{-5}$
Variable Properties (R1)	$1802.338 \pm 7\text{x}10^{-3}$	$3355.072 \pm 7\text{x}10^{-3}$	$3.14424 \pm 1\text{x}10^{-5}$
Variable Properties (R2)	$1802.338 \pm 7\text{x}10^{-3}$	$3139.835 \pm 7\text{x}10^{-3}$	$3.14424 \pm 1\text{x}10^{-5}$

Frozen Flow – mod. 0	$1802.450 \pm 7\text{x}10^{-3}$	$3139.920 \pm 7\text{x}10^{-3}$	$3.14424 \pm 1\text{x}10^{-5}$
Frozen Flow – mod. 1	$1715.090 \pm 8\text{x}10^{-3}$	$3218.531 \pm 7\text{x}10^{-3}$	$3.18174 \pm 1\text{x}10^{-5}$
Frozen Flow – mod. 2	$1662.928 \pm 9\text{x}10^{-3}$	$3259.770 \pm 7\text{x}10^{-3}$	$3.20535 \pm 1\text{x}10^{-5}$
Frozen Flow – mod. 3, 4, 5 and 7	$1609.141 \pm 9\text{x}10^{-3}$	$3309.743 \pm 7\text{x}10^{-3}$	$3.23078 \pm 2\text{x}10^{-5}$
Frozen Flow – mod. 9 and 10	$1609.185 \pm 9\text{x}10^{-3}$	$3309.720 \pm 7\text{x}10^{-3}$	$3.23076 \pm 2\text{x}10^{-5}$
CEA (frozen flow)	**1607.91**	**3311.4519**	**3.231**
Equilibrium Flow – mod. 0	$1802.45 \pm 2\text{x}10^{-2}$	$3139.92 \pm 2\text{x}10^{-2}$	$3.14424 \pm 4\text{x}10^{-5}$
Equilibrium Flow – mod. 1	$2169.9 \pm 3\text{x}10^{-1}$	$3283.5 \pm 4\text{x}10^{-1}$	$3.0009 \pm 6\text{x}10^{-4}$
Equilibrium Flow – mod. 2	$2344.3 \pm 3\text{x}10^{-1}$	$3356.9 \pm 5\text{x}10^{-1}$	$2.9392 \pm 6\text{x}10^{-4}$
Equilibrium Flow – mod. 3 and 4	$2459.8 \pm 2\text{x}10^{-1}$	$3429.8 \pm 5\text{x}10^{-1}$	$2.9147 \pm 6\text{x}10^{-4}$
Equilibrium Flow – mod. 10	$2460.0 \pm 2\text{x}10^{-1}$	$3429.8 \pm 5\text{x}10^{-1}$	$2.9146 \pm 6\text{x}10^{-4}$
CEA (local equilibrium flow)	**2462.41**	**3432.7056**	**2.986**
Non-equilibrium Flow – mod. 31	$1915.20 \pm 4\text{x}10^{-2}$	$3329.958 \pm 3\text{x}10^{-3}$	$3.04829 \pm 2\text{x}10^{-5}$
Non-equilibrium Flow – mod 32	$1980.9 \pm 1\text{x}10^{-1}$	$3335.89 \pm 1\text{x}10^{-2}$	$3.01833 \pm 4\text{x}10^{-5}$

(R1): Rg = 526.97 J/kg·K; (R2): Rg ≈ 461.53 J/kg·K (equivalent to combustion gases mixture for the ideal model)

Taking into account the numerical error estimates, both six-species and eight-species models present the same results or, at least, the values belong to the same numerical range for frozen and local equilibrium flows. The unique exception is made for local equilibrium exit temperature for which both chemical schemes present only one common value over their result ranges. Based on this, at least for the temperature and pressure ranges found in this work, the effect of using chemical reaction schemes with more than six species is nearly null, having influence only on computational efforts (and CPU time requirements).

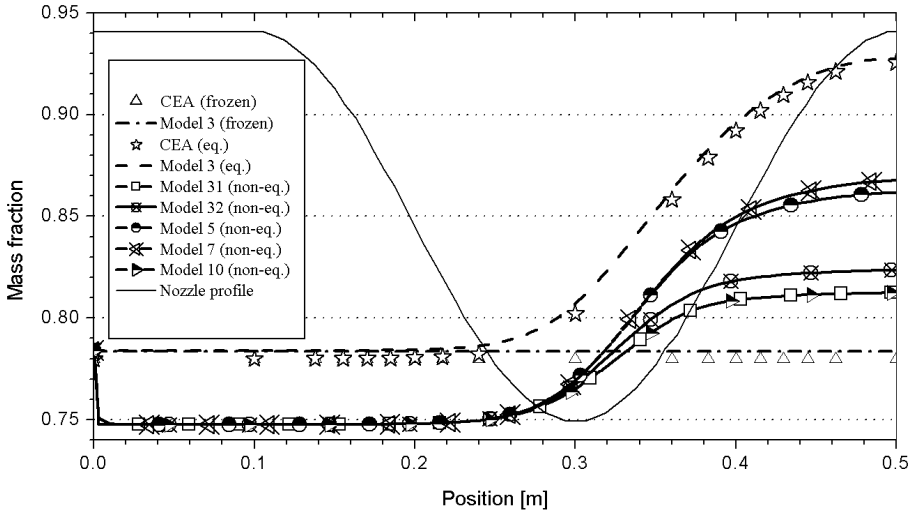

Figure 3. H_2O mass fraction profiles along the nozzle with 80 control volumes.

From Tables 3 to 6, it is seen that non-equilibrium results, as expected, are always between frozen and local equilibrium ones. When the behaviour of thermochemical properties is observed along the whole nozzle structure (Figs. 3 and 4), otherwise, a H_2O mass fraction decrease is observed associated to a temperature drop at the beginning of the flow. It must be noted, nevertheless, that there are significant negative mass generation rates for H_2O, especially for high values of pressure and temperature (it is between $-3.6\text{x}10^5$ and $-4.4\text{x}10^5$ for 3000 K and 2.0 MPa, depending on the chemical model used). Because of this negative mass generation rate, in order to maintain atomic mass conservation, new species must be formed such as O, H and OH. For these new species formation, however, endothermic reactions take place and, therefore, diminish the temperature of the whole gases mixture, as well as the H_2O mass fraction at the beginning of the nozzle structure. It also can be seen that the numerical results of the five chemical schemes present the same numerical results (including the errors estimates) for both C_d and F^*, for 80 control volumes. Because of this, for this grid, any of these chemical schemes can be used.

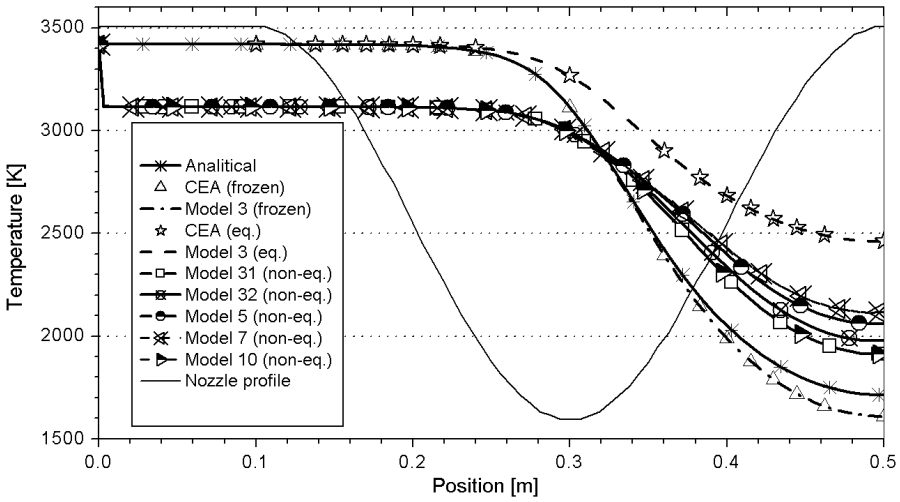

Figure 4. Temperature profiles along the nozzle with 80 control volumes.

6.5 Grid considerations

A last observation is about the grids used in this work: most of the tables and figures show results for 80 control volumes. Even though more refined grids were employed (at maximum, with 10240 control volumes), the 80 control volumes results were preferred. This is because the estimated numerical errors are about the same magnitude of the experimental errors (Marchi et al., 2004). Besides, the CPU time requirement for 80 control volumes is much lower than that for 10240 control volumes (or even a 2560 one). The CPU time consumption for 80 control volumes is at least 40 times lower than that for 2560 control volumes, for isentropic, one-species flow with constant properties (3.1 s against 2.1 min); for equilibrium flow, however, the difference is even greater: it achieves more than 1200 times (2.3 min against 2 days).
For non-equilibrium flow, on the other hand, the differences in CPU time are reduced to about only 6 times (17 min against 1.7 h, for model 31; and 27 min against 2.6 h, for model 32). This reduction in CPU time differences are explained by the reduction in the number of iterations needed for convergence: it was observed that, until the 160 control volumes, for numerical convergence, the number of iterations increase with the grid refinement (as occurred for other physical models); for more refined grids, however, this number of iterations has begun to decrease with grid refinement. Because of this, while for 80 control volumes 5.0×10^6 iterations were needed (for model 31), for 2560 control volumes, only 1.0×10^6 iterations were enough for convergence. Similar behaviour was seen for model 32, in which, for 80 control volumes 1.5×10^7 iterations were used and, for 2560 control volumes, only 1.5×10^6 iterations were necessary.

7 Conclusion

Differently as usually found in literature, the energy equation has the temperature as unknown and not the enthalpy nor the internal energy, as commonly used. Also, the velocity determination is done through the entire engine, covering all the velocity regimes (subsonic, transonic and supersonic ones), and not only the supersonic flow, as commonly done.

Non-equilibrium results, for exit parameters, were always between frozen and local equilibrium ones. However, when the thermochemical profiles along the nozzle structure were studied, a decrease on H_2O mass fraction associated to a temperature drop was verified. A possible explanation for this phenomenon is based on the high negative mass generation rates at conditions of high pressure and high temperature, which allows the appearance of new chemical species, by endothermic chemical reactions, what reduces the gases mixture temperature.

Six and eight-species models have shown the same numerical results for nearly all thermoproperties. Because of this, at least for the temperature and pressure conditions found in this work (until 3400 K and 2.0 MPa), the effect of using chemical reaction schemes with more than six species is nearly null, having influence only on computational efforts. The CPU time requirements present a high variation, especially for local equilibrium flows. The best chemical schemes seemed to be those with lower number of chemical reaction equations. Based on this, models 3 and 4 (six-species models, with four chemical equations) are the most recommendable ones, at least, for preliminary tests.

Most of the results were shown for 80 control volumes, because for this grid the magnitude of estimated numerical errors is equal to experimental ones. Otherwise, the CPU time consumption for 80 control volumes is at least 6 times lower than for 2560 control volumes, achieving a maximum of 1200 times.

8 Acknowledgements

The authors would acknowledge Federal University of Paraná (UFPR), Coordenação de Aperfeiçoamento de Pessoal de Nível Superior (CAPES) and The "UNIESPAÇO Program" of The Brazilian Space Agency (AEB) by physical and financial support given for this work. The first author would, also, acknowledge his professors and friends, by discussions and other forms of support. The second author is scholarship of CNPq (Conselho Nacional de Desenvolvimento Científico e Tecnológico) – Brazil.

9 REFERENCES

Anderson Jr., J. D. Modern Compressive Flow. 2nd ed., McGraw-Hill, New York, 1990.

Barros, J. M. Non-equilibrium Reactive Flow in Convergent Divergent Nozzles [in Portuguese: Escoamento Reativo em Desequilíbrio Químico em Bocais Convergente-Divergente]. M. Sc. Thesis, Technological Aeronautic Institute, São José dos Campos, Brazil, 1993.

Barros, J. E. M.; Alvin Filho, G. F.; Paglione, P. Study of Non-Equilibrium Reactive Flow through Convergent-Divergent Nozzles [in Portuguese: Estudo de Escoamento Reativo em Desequilíbrio Químico através de Bocais Convergente-Divergente]. Proc. 3rd Brazilian Congress of Thermal Engineering and Sciences, Itapema, Brazil, 1990.

Dunn, S. S.; Coats, D. E. Nozzle Performance Predictions Using the TDK 97 Code. Proc. 33rd Joint Propulsion Conference and Exhibit, Seattle, USA, AIAA 97–2807, 1997.

Ferziger, J. H.; Perić, M. Computational Methods for Fluid Dynamics. 3 ed. Berlin: Springer-Verlag, 2001.

Fröhlich, A.; Popp, M.; Schmidt, G.; Thelemann, D. Heat transfer characteristics of H_2/O_2 combustion chambers. In: 29th Joint Propulsion Conference. Monterrey: Proceedings… AIAA 93 – 1826, 1993.

Glenn Research Center. CEA – Chemical Equilibrium with Applications. Available in: <http://www.grc.nasa.gov/WWW/CEA Web/ceaHome.htm>. Access in: Feb 16, 2005.

Kee, R. J.; GrCar, J. F.; Smooke, M. D.; Miller, J. A. A Fortran Program for Modeling Steady Laminar One-Dimensional Premixed Flames. Albuquerque: Sandia National Laboratories. SAND85-8240 · UC-401, 1990.

Kee, R. J.; Rupley, F. M.; Meeks, E.; Miller, J. A. Chemkin-III: A Fortran Chemical Kinetics Package for the Analysis of Gas-Phase Chemical and Plasma Kinetics. Albuquerque: Sandia National Laboratories, SAND96-8216 · UC-405, 1996.

Kuo, K. K. Principles of Combustion. John Wiley & Sons, New York, 1986.

Laroca, F. Reactive Flow Solution in Expansion Nozzles Using the Finite Volume Method [in Portuguese: Solução de escoamentos reativos em bocais de expansão usando o método dos volumes finitos]. M. Eng. Thesis, Santa Catarina Federal University, Florianópolis, Brazil, 2000.

Marchi, C. H. Verification of One-Dimensional Numerical Solutions in Fluid Dynamics [in Portuguese: Verificação de Soluções Numéricas Unidimensionais em Dinâmica dos Fluidos]. PhD Thesis, Federal University of Santa Catarina, Florianópolis, Brazil, 2001.

Marchi, C. H.; Laroca, F.; Silva, A. F. C.;Hinckel, J. N. Numerical Solution of Flows in Rocket Engines with Regenerative Cooling [in Portuguese: Solução Numérica de Escoamentos em Motor-Foguete com Refrigeração Regenerativa]: Proc. 21st Iberian Latin American Congress on Computational Methods in Engineering, Rio de Janeiro, Brazil, 2000.

Marchi, C. H.; Laroca, F.; Silva, A. F. C.; Hinckel, J. N. Numerical solutions of flows in rocket engines with regenerative cooling. Numerical Heat Transfer, Part A, v. 45, pp. 699 – 717, 2004.

Marchi, C. H.; Maliska, C. R. A nonorthogonal finite volume method for the solution of all speed flows using co-located variables. Numerical Heat Transfer, Part B, v. 26, pp. 293 – 311, 1994.

Marchi, C. H.; Silva, A. F. C. Unidimensional numerical solution error estimation for convergent apparent order. Numerical Heat Transfer, Part B, v. 42. pp. 167–188, 2002.

Roache, P. J. Perspective: A method for uniform reporting of grid refinement studies. Journal of Fluids Engineering, v. 116, pp. 405-413, 1994.

Smith, T. A.; Pavli, A. J.; Kacynski, K. J. Comparison of theoretical and experimental thrust performance of a 1030:1 area ratio rocket nozzle at a chamber pressure of 2413 kN/m^2(350 psia). Cleveland: NASA Lewis Research Center. NASA Technical Paper 2725, 1987.

Sutton, G. P.; Biblarz, O. Rocket Propulsion Elements. 7 ed. New York: John Wiley & Sons.

Svehla, R. A., 1964. Thermodynamic and transport properties for the hydrogen-oxygen system. Cleveland: NASA Lewis Research Center. NASA SP-3011, 2001.

Tannehill, J. C.; Anderson, D.; Pletcher, R. H. Computational Fluid Mechanics and Heat Transfer. 2 ed. Philadelphia: Taylor & Francis, 1997.

Van Doormaal, J. P.; Raithby, G. D. Enhancements of the SIMPLE method for predicting incompressible fluid flow. Numerical Heat Transfer, v. 7, pp. 147 – 163, 1984.